Solution processable titanium dioxide precursor and nanoparticulated ink: Application in Dye Sensitized Solar Cells

Pau Bosch-Jimenez [a], Youhai Yu [b], Mónica Lira-Cantu [b], Concepción Domingo [c], José A. Ayllón [a,⇑]

[a] Departament de Química, Universitat Autònoma de Barcelona, Campus UAB, 08193 Bellaterra, Spain

[b] Centre d'Investigació en Nanociència i Nanotecnologia (CIN2, CSIC-ICN), Campus UAB, 08193 Bellaterra, Spain

[c] Institut de Ciència dels Materials de Barcelona (CSIC), Campus UAB, 08193 Bellaterra, Spain

Keywords:
Titanium dioxide
Dye Sensitized Solar Cells (DSSCs)
Proton Nuclear Magnetic Resonance (^{1}H NMR)
Nanoparticles
Ink
Low-temperature

a b s t r a c t

Colloidal TiO_2 anatase nanoparticles of 4–8 nm diameter capped with 3,6,9-trioxadecanoic acid (TODA) were synthesized at low temperature using water and ethanol as the solvents. ATR-FTIR and ^{1}H NMR characterization showed the capping acid capability of stabilizing the TiO_2 nanoparticles through labile hydrogen bonds. The presence of the capping ligand permitted the further preparation of homogeneous and stable colloidal dispersions of the TiO_2 powder in aqueous media. Moreover, after solvent evaporation, the ligand could be easily eliminated by soft treatments, such as UV irradiation or low-temperature thermal annealing. These properties have been used in this work to fabricate mesoporous TiO_2 electrodes, which can be applied as photoanodes in Dye Sensitized Solar Cells (DSSCs). For the preparation of the electrodes, the as-synthesized mesoporous TiO_2 nanoparticles were mixed with commercial TiO_2 (Degussa P25) and deposited on FTO substrates by using the doctor blade technique. A mixture of water and ethanol was used as the solvent. A soft thermal treatment at 140 C for 2 h eliminated the organic compound and produced a sintered mesoporous layer of 6 lm thickness. The photovoltaic performance of the DSSCs applying these electrodes sensitized with the N3 dye resulted in 5.6% power conversion efficiency.

1. Introduction

The increasing world energy demand and the problems associated with fossil fuels highlight the need to develop clean, sustainable and economically viable alternatives, such as solar cells. A key issue in this scenario is to have a technology capable of producing a large number of solar cells in a short time and with a low energy payback time (EPT) [1]. Dye Sensitized Solar Cell (DSSC) is a prospective solution to convert solar power into useful electrical energy. The great interest in this type of solar cells is justified by the important potential advantages over other photovoltaic technologies: low production cost, low EPT, use of materials of standard purity, good efficiency under diffuse light and at high temperatures, and adaptability to a large diversity of designs (transparency, colorful, flexible, lightweight, bifacial cells, etc.) that would facilitate their integration into buildings or appliances [2,3]. However, in order to be competitive with current inorganic solar cells, DSSC technology must increase power conversion efficiency, reduce fabrication cost and increase lifetime. The reduction of fabrication costs requires a cutback in the environmental and economic costs [4].

Low temperature procedures, involving the elimination of the sintering steps of the TiO_2 electrode at high temperature (450 C), could be advantageous to achieve this objective. Currently, TiO_2 DSSCs showing record efficiencies in the order of 12% require two annealing steps at high temperature, the second one after treatment of the TiO_2 mesoporous layer with a $TiCl_4$ solution [5,6]. Low temperature processed electrodes results in DSSCs with lower power conversion efficiency [7–12] and mechanical stability than electrodes sintered at high temperature [13]. Some of the main drawbacks observed in TiO_2 electrodes fabricated at lowtemperature are variable quality of the film due to irregular distribution of the nanomaterial in the film and appearance of cracks, voids or pinholes that are mainly originated by an inadequate or inhomogeneous texture of the TiO_2 precursor paste [13]. To design low-temperature fabrication efficient methods of TiO_2 electrodes, the use of high boiling temperature organic compounds should be avoided. Hence, the use of water and/or ethanol user-friendly solvents to the formulation of TiO_2 inks is desirable. Other volatile additives applied in low quantity, such as HCl or NH_3, can also be added; but organic compounds with high boiling points, frequently used as additives to control the viscosity of the paste and the porosity of the resulting film, must be avoided [14,15]. On the other hand, the intimate contact between nanoparticles is mandatory to reach a good electron transport, but it is hard to achieve in processes performed at low temperature. An attractive alternative to increase nanoparticles contact introduced by Hagfeld et al. [16] was the application of high pressure on the film, resulting in increased DSSCs efficiencies up to 7.6% [17,18].

A different explored strategy consists in the fabrication of colloidal TiO_2 pastes involving a mixture of preformed anatase nanoparticles and a molecular TiO_2 precursor [19,20]. After a thermal or UV treatment, the molecular TiO_2 precursor is transformed into nanocrystallites of TiO_2 that act as cement between the different nanoparticles. In this route, the thermal sintering is replaced by a chemical process, in which the connection between nanoparticles is done by deposition of additional TiO_2 [21]. The easiest developed methodology consists in the use of a mixture of a titanium(IV) alcoxide precursor and preformed TiO_2 nanoparticles [8,9,22]. However, this route has the shortcoming of the difficulty of controlling the degree of alcoxide hydrolysis during the manipulation and/or storage of the paste. In a similar approach, the titanium molecular precursor is replaced by small size titania nanoparticles (<10 nm) that act as a glue due to its great tendency to aggregate and to get anchored to the larger titania nanoparticles [23,24].

Without surface ligands, colloidal nanoparticles have a strong tendency to aggregate, which is accentuated as the particle size is reduced. Surface modification of inorganic colloids with organic ligands is a common method applied to facilitate further processing as inks. The coating allows thin film deposition from colloidal dispersions by different processes, such as spring-coating, ink-jet printing [25–27]. Particularly, TiO_2 thin films have a wide

Corresponding author. Fax: +34 93 581 2176.
E-mail address: joseantonio.ayllon@uab.es (J.A. Ayllón).

range of applications as optical coatings, gas sensors, protective layers of transparent conductive coatings and in optoelectronic devices, catalytic processes, etc. Therefore, easily processable colloidal TiO_2 ink is a focal material to develop. The stability of colloidal dispersions in different solvents is determined by the nature of the ligands anchored to their surface. On the other hand, the presence of capping ligands could be a drawback for many applications that require a close contact between deposited nanoparticles. Frequently, a thermal processing at high temperature is necessary to remove the organic coating and to allow for the direct contact between nanoparticles, which limits both the materials and the processes that can be used [28,29].

In this work, the use of 3,6,9-trioxadecanoic acid (TODA) as a capping ligand for TiO_2 is described. This ligand has sufficient affinity to the titania surface to stabilize the nanoparticles as a colloidal dispersion in aqueous solvents. Moreover, the capping agent can be easily removed with a simple and smooth post-treatment. This precursor is further applied in the formulation of colloidal inks, which permit the preparation of TiO_2 mesoporous layers at low temperature to be employed as photoanodes in DSSCs.

2. Experimental methods

2.1. Reagents

All chemicals used in this work were commercially available and were used without further purification: titanium(IV) isopropoxide (TTIP, 97%, Aldrich), 3,6,9-trioxadecanoic acid (TODA, 98.4%, Aldrich), hydrochloric acid (HCl, 37%, Panreac) and ethanol (EtOH, 99.5%, Panreac). TiO_2 Degussa P-25 (80% anatase–20% rutile) was kindly gifted by Degussa (Spanish delegation). Ultra pure water (Milli-Q system, conductivity lower than 0.05 lS cm^1) was used.

2.2. TODA@TiO_2 nanoparticles synthesis

TODA (0.301 g, 1.66 mmols) was dissolved in ethanol (40 mL) and 1.0 mL of hydrochloric acid (37%) was added. Then, titanium isopropoxide (5 mL, 16.9 mmols) was added and a clear solution was obtained after moderate agitation. This solution was slowly added over a reactor containing boiling water (250 mL). The volume of the clear suspension so obtained was reduced to 40 mL by solvent evaporation at boiling temperature. The recovered white suspension was then ultrasonicated during 25 min to obtain a slightly yellow translucent suspension. The white solid material was isolated from the suspension by slow water evaporation at 50 C. The recovered solid residue was crushed in a mortar and treated as a water redispersible powder. The TiO_2 percentage by weight was estimated as 78% by measuring the weight reduction after annealing (30 min at 450 C). The concentrated translucent colloidal solution obtained after sonication was used either as obtained or diluted with ethanol (3 mL ethanol for each 1 mL of colloidal suspension) to deposit thin films by spin-coating.

2.3. TiO_2 ink formulation

The optimized composition includes a mixture of 0.750 g of solid TODA@TiO_2 powder and 1.750 g of TiO_2 Degussa P25. The combined solids were suspended in a mixture of 3 mL of H_2O and 2 mL of EtOH.

2.4. Solar cell fabrication

The FTO glass (Solems SnO_2:F, 7–10 ohm/sq) was first cleaned for 20 min in a detergent aqueous solution (Empigem BB, Aldrich) using an ultrasonic bath, then rinsed with ultra pure water and ethanol and dried under N_2 flux. Finally, it was cleaned for 20 min in a UV-O_3 surface decontamination system (Novascan, PSD-UV, Novascan, IA, USA) connected to an oxygen gas source. TiO_2 porous layers were deposited by doctor blade technique. After drying at room temperature, different treatments were studied to promote the sinterization of the pre-formed TiO_2 layer: thermal treatment and/or UV light irradiation. The heating was performed in a conventional oven with forced ventilation at temperatures in the 90–140 C range. For ultraviolet irradiation treatment, films were located at 8 cm from a medium-pressure Hg lamp (125 W, HPK Cathodeon) and no filter was placed between the lamp and the sample. The electrodes were immersed into a 0.5 mM solution of N3 dye (Greatcell Solar S.A.) in ethanol and kept at room temperature for 24 h to assure complete sensitizer uptake. The dye-sensitized TiO_2 films were rinsed with acetone and dried under nitrogen before being used. A Pt back electrode (made by e-beam deposition) was attached by the Surlyn hot-press film. The final active area was 0.2 cm^2. The electrolyte Iodolyte AN-50 and the N-719 dye, were all purchased from Solaronix.

2.5. Characterization

XRD spectra were recorded on a Rigaku Rotaflex RU-200B diffractometer with Cu Ka radiation (k = 1.5418 Å). Ultraviolet–visible (UV–vis) spectroscopy was performed using a UV Hekios c Thermo Electron Corporation spectrophotometer. Aqueous suspensions were used to register the UV–Vis absorption spectra of the nanoparticulated samples. Attenuated total reflectance Fourier transform infrared (ATR-FTIR) spectra were recorded in a Perkin Elmer apparatus (Spectrum One, model equipped with a Universal ATR Sampling Accessory). ^{1}H NMR spectra were recorded on an NMR-FT Bruker AC-250 MHz spectrometer in D_2O; chemical shifts are referenced to the residual proton signal of the deuterated solvent and are given in ppm. SEM images were recorded with a Zeiss Merlin FE-SEM microscope operating at 1 kV. EDX Electron-diffraction patterns and high-resolution transmission electron microscopy (HR-TEM) images were recorded in a JEOL 2011 microscope operated at 200 kV. Textural properties of the porous TiO_2 layer were studied by low-temperature N_2 adsorption analysis (ASAP 2000 Micromeritics). Prior to measurements, samples were dried under reduced pressure (<1 mPa) at 393 K for 18 h. Specific surface area (S_a) values were determined from the adsorption branch of the isotherms by the BET method.

The solar simulation was carried out with a Steuernagel Solarkonstant KHS1200 equipped with an AM1.5 filter for all characterization (1000 W/m^2, AM1.5G). Light intensity was 1000 W/m^2 calibrated with a Zipp & Konen CM-4 pyranometer, which is used constantly during measurements to set light intensity together with a calibrated Si solar cell from NREL. The sun simulator was calibrated with a calibrated photodiode from Hamamatsu and a mini spectrophotometer from Ava-Spec 4200. The AM1.5G reference spectrum agreed with the ASTM G173 standard. IV-curves were measured using a Keithley 2601 multimeter connected to a computer and controlled with the SolarCEll_v4_SP software developed by Mikkel Jorgensen at RISO-DTU. IPCE analyses were carried out with a QE/IPCE measurement system from Oriel at 10 nm intervals from 300 to 800 nm. The IPCE equipment was calibrated before measurements with a S1227-1010BQ photodiode from Hamamatsu. The results were not corrected for intensity losses due to light absorption and reflection by the glass support.

3. Results and discussion

TODA capped TiO_2 nanoparticles (TODA@TiO_2) were obtained by hydrolysis of titanium isopropoxide in an ethanol–water solution of the carboxylic acid. A 10:1 TTIP:TODA molar ratio was used. A smaller proportion of TODA was not enough to stabilize the nanoparticles adequately. Due to the high stability of the prepared suspension, the TiO_2 nanoparticles could not be isolated satisfactorily by filtration or centrifugation. Therefore, the solvent was removed by evaporation at low temperature (50 C) until a solid residue was obtained, which was then crushed by hand in an agate mortar. A fine powdered material, easily redispersible in water, was obtained. XRD pattern (Fig. 1a) shows that this material contains poorly crystallized titanium dioxide. When hydrochloric acid was added to the initial reaction mixture, the crystallization of TiO_2 was enhanced (Fig. 1b). Anatase was the main precipitated phase, although

small traces of brookite were also present. A 7.5 nm particle size was estimated for this material using the Scherrer's equation (101 peak). Crystal growth and/or aggregation were likely limited by the anchoring of TODA to the surface of the TiO_2 and, consequently, nanometric particles were produced.

Hydrolysis in acid medium of a solution of Ti:TODA with a 10:1 M ratio was fixed as the processing route for the synthesis of the optimized nanoparticulated material labeled TODA@TiO_2, which was, after characterization, used in further processing. UV/VIS spectrum (Fig. 2) shows the characteristic tail of the absorbance of crystalline TiO_2. The estimated E_{BG} value, 3.2 eV, matched the value of anatase (inset Fig. 2) [30]. This material has a TiO_2 percentage of 78wt%, value that is in agreement with the calculated by considering that the titanium alcoxide was quantitatively hydrolyzed to titanium dioxide and that all added TODA remained adsorbed on the solid.

TEM and HR-TEM micrographs (Fig. 3) show that the TODA@TiO_2 nanoparticles form aggregates. Fringes corresponding to crystalline planes are observed in most of the crystallites of 4– 8 nm size, which are in intimate contact with each other. SAED analysis (Fig. 3c) confirmed also the crystalline nature of the titania nanoparticles, rings corresponding to the (101), (004) and (200) planes of anatase being clearly defined. These observations concur with XRD data. It is interesting to remark that the aqueous diluted dispersion used to prepare the TEM sample was completely transparent to the eye which indicated that the TODA@TiO_2 nanoparticles had a very low degree of aggregation in water. The strong aggregation visible in the TEM micrographs must be caused by the evaporation of the solvent and possibly also by TODA desorption from the surface of TiO_2 at high vacuum. This fact suggests that the grafting between TODA and titanium dioxide was relatively labile.

The polar tail of TODA, with three ether groups, facilitates the dispersability of TODA@TiO_2 in water. However, the key point to gain insight in the way TODA stabilizes the nanoparticles dispersion is to ascertain how TODA is anchored to de titania surface. Carboxylic acids can bond to metallic oxides through different modes of coordination of the carboxylate group (ACOO) [31] or via hydrogen bond between the protons of the carboxylic acid and the oxygen atoms on the surface of the oxide [32]. Moreover, interaction is also possible between carbonyl oxygen and the hydroxyl groups on the oxide surface [33,34]. A carboxylate coordination type has been clearly established in the literature for TiO_2

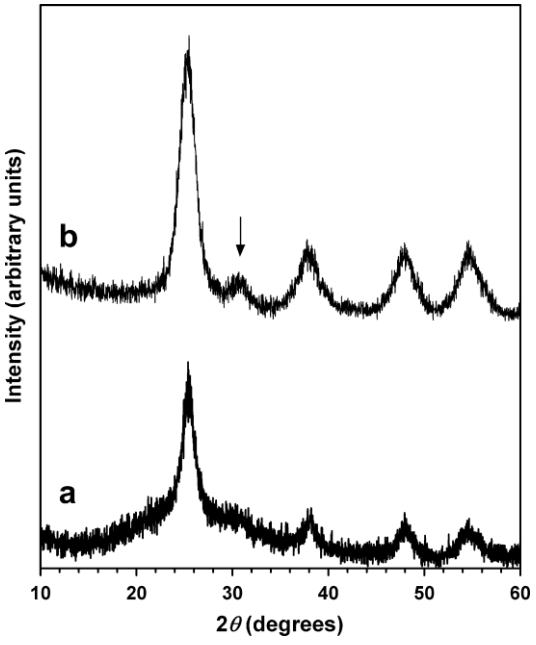

Fig. 1. Powder XRD pattern of the material prepared with TODA as surface modifier: (a) without added acid, and (b) with added acid. All peaks could be assigned to anatase (JCPDS No. 21-1272), except the marked peak that corresponded to traces of brookite.

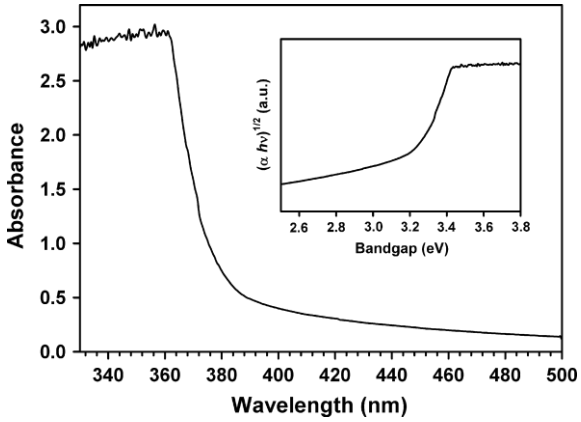

Fig. 2. UV–vis absorption spectrum of TODA@TiO_2 nanoparticles (solvent: water). Inset: plot of the transformed Kubelka–Munk function vs. the energy of absorbed light.

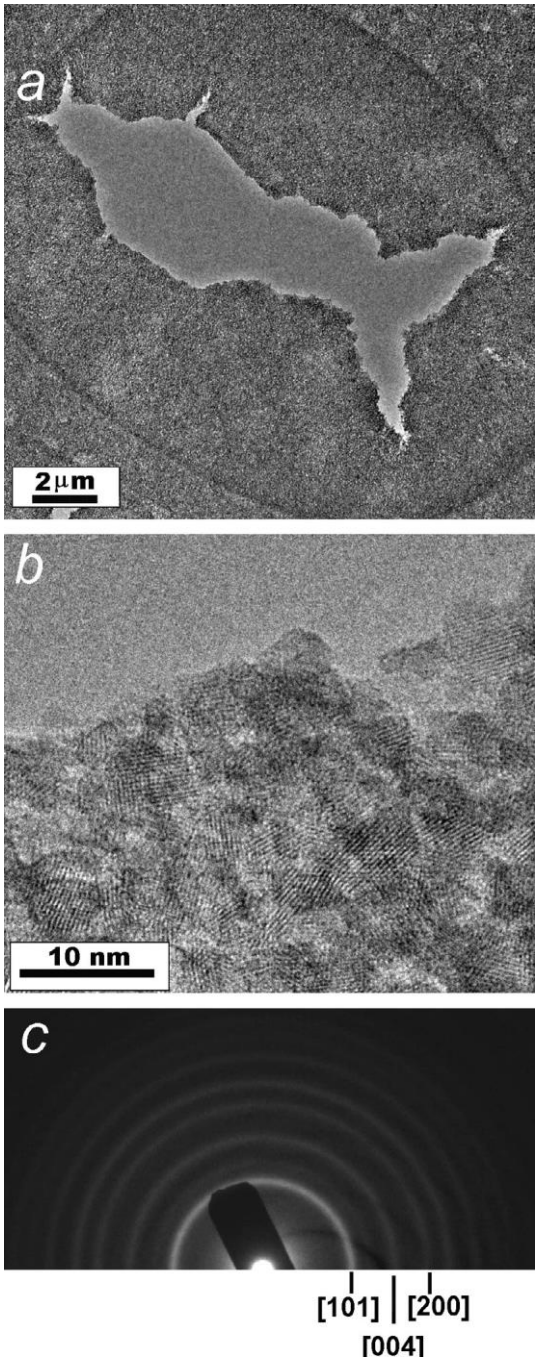

Fig. 3. (a and b) TEM and HR-TEM micrographs of: TODA@TiO_2 nanoparticles at different magnification, and (c) selected area electron diffraction spectrum.

nanoparticles prepared using organic solvents in absence of water and using carboxylic acid with a hydrophobic tail, as for instance dodecanoic or oleic acid [34,35]. A priori, the use in the method described in this work of an acidic aqueous medium should favor that TODA remains as protonated carboxylic acid; but, on the other hand, the fact that a nanostructured material easily dispersible in water was obtained implies that TODA molecules are efficiently anchored on the TiO_2 surface.

Infrared spectroscopy was primarily used to ascertain the coordination mode of carboxylate modified nanoparticles. ATR-FTIR spectrum of TODA@TiO_2 nanoparticles is shown in Fig. 4a. The band at 1723 cm^1 was assigned to the vibration of the protonated carboxylic acid in TODA and probes the presence of a significant

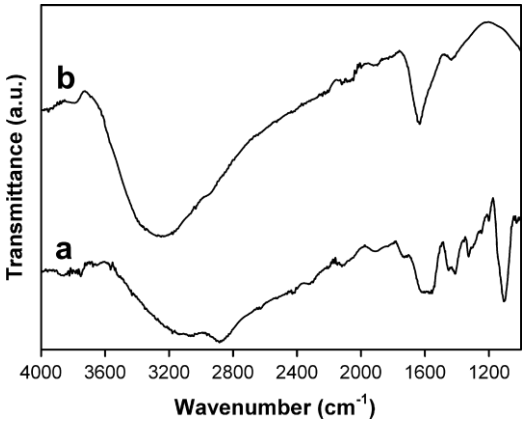

Fig. 4. FT-IR spectrum of (a) TODA@TiO_2 solid powder sampled and (b) a sample from a TiO_2 film treated at 140 C for 2 h-algo falla- a sample from a porous layer treated at 140 C during 2 h.

proportion of this specie on the solid surface. The spectrum reveals relatively bad defined broad bands in comparison with other TODA capped nanoparticles reported in the literature [31,36], indicative of a mixture of different TODA coordination modes. This broadening, and the overlap of the bands due to H_2O bending and C@O stretching, make it difficult to precise the carbonyl position and, thus, to use this value to ascertain the TODA coordination mode on TiO_2 surface. The broad band centered at 3100 cm^1 sum up vibrations of OAH stretching from adsorbed water, COOAH and hydroxyl groups on the surface of TiO_2. The band at 2855 cm^1 (CAH stretching) was assigned to the methylene groups. The band at 1097 cm^1 corresponded to the vibration of the CAOAC stretching [31].

Taking advantage of the easy dispersibility of the prepared TODA@TiO_2 material in water, it was further characterized by ^{1}H NMR. The spectra of the sodium salt of TODA (Fig. 5a), pure TODA (Fig. 5b) and TODA@TiO_2 nanoparticles (Fig. 5c) were recorded in

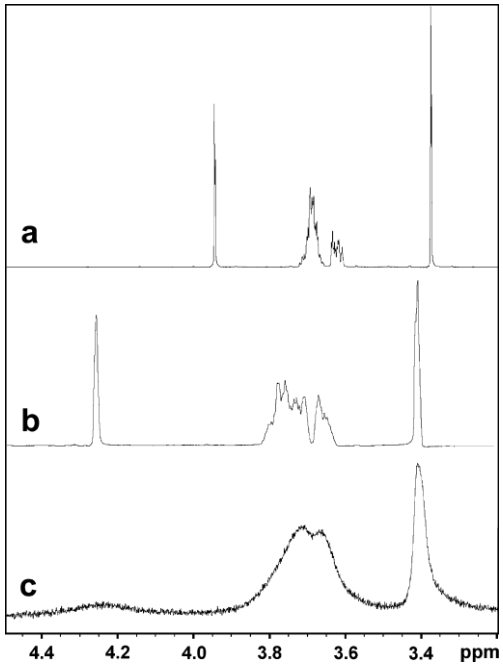

Fig. 5. ^{1}H RMN of: (a) sodium salt of TODA, (b) pure TODA, and (c) TODA@TiO_2 nanoparticles. Inset: magnification of the broad signal of spectrum (c). In all samples solvent was D_2O.

deuterated water. In all three cases, the signal that appeared at around 3.4 ppm corresponded to the three protons of the terminal methyl group. The signals between 3.6 and 3.8 ppm belong to the eight protons in the $OACH_2ACH_2AO$

groups. The position of these signals in the colloid was more similar to the position in the pure TODA than in the sodium salt. The most notable differences between the three studied samples were observed in the signal corresponding to the two protons of the CH_2 group next to the carboxylic functionality. For pure TODA, this signal appeared at 4.26 ppm, whereas in the spectrum of the sodium salt it was located at 3.96 ppm, being this position similar to that reported by Barron et al. [37], for deprotonated TODA capping alumoxane. The ^{1}H NMR spectrum of the colloid TODA@TiO_2 nanoparticles showed a very wide signal centered at 4.25 ppm, a position almost equal to the one corresponding to the CH_2 group directly bonded to the protonated carboxyl group in pure TODA. The widening of the peaks was caused by a restricted rotational mobility, since TODA was adsorbed on the surface of TiO_2 and, probably, also by the existence of dynamic processes related to adsorbate mobility and/or exchange equilibrium. The different degree of peaks broadening reflects that the strongest interactions between TODA and the nanoparticles surface are established through the carboxylic acid group [38,39], most likely through hydrogen-bond interactions [32]. Moreover, this is a reasonable conclusion considering the instability in the presence of water of the carboxylate ester type grafted on the TiO_2 surface [34]. Recently, Grote et al. has reported that even a weak interaction between an organic compound and the nanoparticles surface can generate stable colloidal dispersions [40].

Thin layers were deposited on FTO substrates by spin coating of a suspension of TODA@TiO_2 nanoparticles. The aqueous suspension was not the adequate medium to produce homogeneous thin films, since it did not wet properly the FTO substrate. Hence, an optimized solvent involving ethanol and water in a ratio EtOH:H_2O 3:1 v/v was used to obtain homogenous thin films. After applying a soft thermal treatment with either UV irradiation (15 min) or heating at 120–140 C, the obtained TiO_2 layers showed high adhesion on FTO glass substrates, since they remained attached to them even after being subjected to ultrasonic bath treatment (10 min). Furthermore, deposited films were very homogenous, transparent and colorless. Cross-sectional images of the layers obtained with backscattered electrons showed a thin film (100–200 nm) of TiO_2 deposited on the FTO (Fig. S1). EDX analysis verified that the layer was composed of titanium dioxide, as it was previously inferred from the UV/VIS spectrum of the thin film (Fig. S2).

In order to apply the precursor developed in this work to prepare thick TiO_2 films (in a single step), useful to fabricate DSSCs, an ink based on the concept of ‘‘bricks and cement’’ was developed. TiO_2 Degussa P25 nanoparticles were used as the bricks, while the cement or glue was the TODA@TiO_2 nanoparticulated dispersion. The ink was optimized by first varying the amount of the two TiO_2 materials involved in the formulation and by using different mixtures of water and ethanol as the solvent. The presence of cracks and inhomogeneities (pores and macroscopic lumps) were qualitatively used to evaluate the formulation. The optimized ink contains 30wt% of TODA@TiO_2 and 70wt% of TiO_2 Degussa P25. A mixture in volume consisting of three parts of water for every two parts of ethanol (H_2O:EtOH 3:2 v:v) was used as a dispersion medium with a total solid load of 500 mg mL^{-1}. A similar strategy has been recently reported by Ko et al. [23,24], however, details of the synthesis of the nanoparticles used as a ‘‘nanoglue’’ are not given.

For comparison purposes, solar cells applying the same TiO_2 ink, but annealed at conventional high temperature (450 C for 30 min), was made. In this case, the photovoltaic response was of 7.1% power conversion efficiency. This reference value was basically limited by the thickness of the TiO_2 layer; a value close to

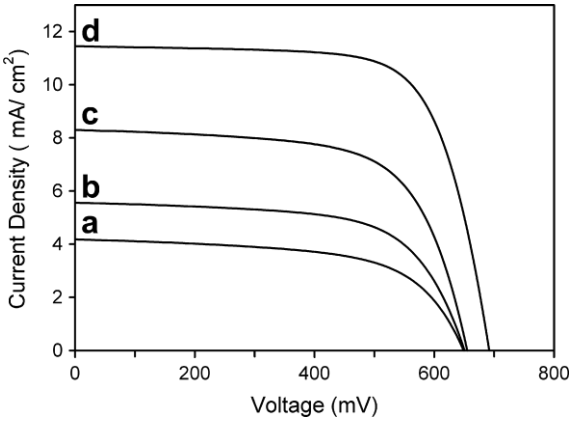

Fig. 6. I–V curves obtained for representative DSSC devices.

12 lm is optimal for a DSSC with a N3 dye-electrolyte system [41]. The formulation of the paste determined the thickness of the mesoporous layer. The increase in the solid loading resulted in a thicker layer, but this option was discarded as a method of increasing the efficiency because the deposited film has cracks and inhomogeneities.

Once the composition of the ink was fixed, different treatments were studied in order to promote the elimination of the TODA additive, and thus, the chemical sinterization of the mesoporous layer. Irradiation with ultraviolet light (UV) resulted in DSSCs with efficiencies of 1.6% and 2.3% for 1 and 3 h treatment, respectively (Fig. 6 curves a and b). Power conversion efficiency was increased up to 3.6% by combining thermal treatment (120 C for 60 min) and UV radiation (60 min), as shown in Fig. 6 curve c. Combined treatment shows an increase in power conversion efficiency with respect to both thermal at 120 C and UV radiation. However, it results in lower efficiency if compared to that obtained by applying only heat treatment at the slightly higher temperature of 140 C (Fig. 6 d). At 140 C, an efficiency of 5.6% was attained. Layers obtained at 140 C showed the highest adhesion to the FTO substrate, evaluated according to the amount of material that remained attached after been submerged in water in an ultrasound bath. Other relevant DSSC parameters measured as a function of the TiO_2 layer post-treatment are summarized in Table 1.

The images provided by SEM (Fig. 7) show that the mesoporous layer was homogeneous and without cracks (Fig. 7a). Fig. 7b shows that the layer consists of TiO_2 nanoparticles of different sizes which are well connected and forming a structure with high porosity. Transverse micrographs of the layer were used to estimate a thickness in the order of 6.0 lm (Fig. 7c). The layer was also homogeneous in the transverse direction.

The textural properties of the optimized TiO_2 layer were characterized by low-temperature N_2 adsorption/desorption analysis (Fig. 8). A specific surface area of 94 $m^2 g^{-1}$ was determined, a value clearly higher than the surface area of the TiO_2 Degussa P25 (50 $m^2 g^{-1}$), indicating that the small TiO_2 nanoparticles from TODA@TiO_2 were bounded to the surface of the TiO_2 Degussa

Table 1
Effects on DSSC parameters of the different treatments performed to the TiO_2 layer.

Parameter	Treatment			
	UV, 1 h	UV, 3 h	UV, 1 h + 120 C, 1 h	140 C, 2 h
J_{sc} (mA cm^{-2})	4.18	5.56	8.30	11.45
V_{oc} (V)	0.65	0.65	0.66	0.69
FF (%)	61.05	64.22	65.53	71.30
g (%)	1.6	2.3	3.5	5.6

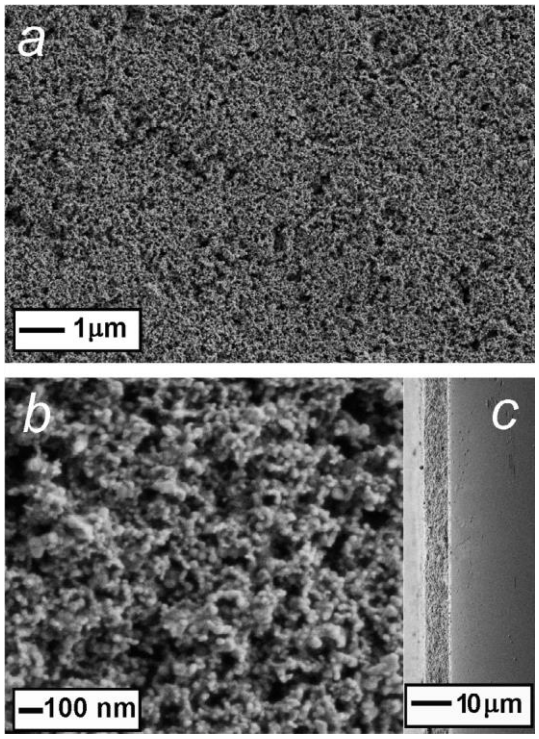

Fig. 7. SEM micrographs of the TiO_2 layer obtained after the treatment at 140 C for 2 h: (a and b) surface, and (c) transversal cut.

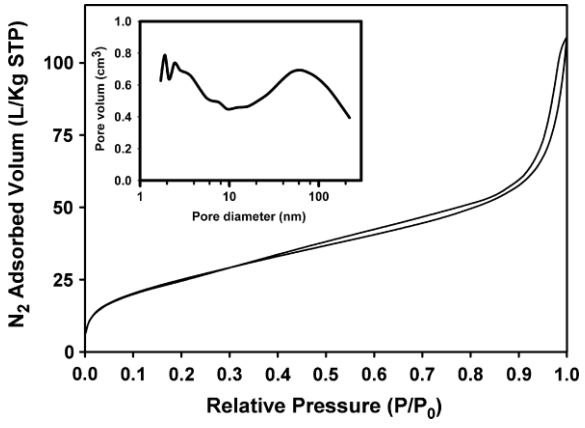

Fig. 8. Low temperature nitrogen adsorption–desorption isotherms and pore size distribution, calculated from the adsorption branch of the isotherm, (inset) of a sample obtained by submitting the TiO_2 layer at 140 C for 2 h.

P25 nanoparticles, thus increasing the roughness and, consequently, the surface area. A Type IV adsorption isotherm was recorded, which corresponds to a mesoporous solid with a small percentage of micropores. At relatively high pressures, the isotherm developed a small hysteresis that can be classified as type H1 with easily accessible pores. The pore size distribution (inset in Fig. 8) was wide, being a significant portion of it mesopores (2–50 nm) and only some of them micro (<2 nm) or macroporous (>50 nm). The uneven distribution of pore sizes is suitable for use in DSSC electrodes, as it would allow for an easy access of the dye and electrolyte to the internal surface of TiO_2.

Comparing the ATR-FTIR spectra of the material obtained after subjecting the mesoporous layer at 140 C for 2 h and the TODA@TiO_2 as-synthesized nanoparticles (Fig. 4b), it can be observed the almost total disappearance of the TODA characteristic bands. Only the broad band centered at 3240 cm^1 and the band at 1627 cm^1 remained, both assigned to adsorbed water. Hence, the mild thermal treatment eliminates the organic matter from the surface of TiO_2 nanoparticles, producing a sintering effect.

4. Conclusions

The main aim of this work has been the development of a colloidal TiO_2 ink that facilitates the low temperature manufacturing of DSSC photoanodes. The key component was a TiO_2 colloid stabilized in aqueous media with the help of 3,6,9-trioxadecanoic acid, which was anchored on the titania colloid through labile hydrogen bonds. The bond is strong enough to allow the nanoparticles to form stable suspensions in water, but weak enough to allow TODA elimination when subjecting the dry material to high vacuum or to a soft thermal treatment (140 C). The optimized ink has a simple composition, high stability, homogeneity, wets FTO well and has no lumps; properties that allow obtaining homogeneous mesoporous TiO_2 layers by doctor blade method. The thermal treatment induces the small 4–8 nm TODA@TiO_2 nanoparticles to link with TiO_2 P25 NP, which increases the connections between both type of particles and allows the sintering and formation of a mesoporous titanium oxide layer. DSSCs with an efficiency as high as 5.6% were obtained in this way.

Acknowledgment

The work described in this paper was supported by the Spanish National Plan of Research (MAT2012-35161). Authors are grateful to Dr. Ramón Alibes and Dr. Antoni Figueras for their help in measuring the NMR spectra.

References

[1] N.S. Lewis, Science 315 (2007) 798–801.
[2] M.K. Nazeeruddin, E. Baranoff, M. Gratzel, Sol. Energy 85 (2011) 1172–1178.
[3] S. Zhang, X. Yang, Y. Numata, L. Han, Ener. Environ. Sci. 6 (2013) 1443–1464.
[4] M. Graetzel, R.A.J. Janssen, D.B. Mitzi, E.H. Sargent, Nature 488 (2012) 304–312.
[5] B.C. O'Regan, J.R. Durrant, P.M. Sommeling, N.J. Bakker, J. Phys. Chem. C 111 (2007) 14001–14010.
[6] P.M. Sommeling, B.C. O'Regan, R.R. Haswell, H.J.P. Smit, N.J. Bakker, J.J.T. Smits, J.M. Kroon, J.A.M. van Roosmalen, J. Phys. Chem. B 110 (2006) 19191–19197.
[7] Y.J. Chen, E. Stathatos, D.D. Dionysiou, J. Photochem. Photobiol., A 203 (2009) 192–198.
[8] A. Du Pasquier, Electrochim. Acta 52 (2007) 7469–7474.
[9] K. Fan, T.Y. Peng, J.N. Chen, K. Dai, J. Power Sources 196 (2011) 2939–2944.
[10] K. Kim, G.W. Lee, K. Yoo, D.Y. Kim, J.K. Kim, N.G. Park, J. Photochem. Photobiol. A 204 (2009) 144–147.
[11] Z. Tebby, O. Babot, D. Michau, L. Hirsch, L. Carlos, T. Toupance, J. Photochem. Photobiol. A-Chem. 205 (2009) 70–76.
[12] D. Zhao, T.Y. Peng, L.L. Lu, P. Cai, P. Jiang, Z.Q. Bian, J. Phys. Chem. C 112 (2008) 8486–8494.
[13] H.C. Weerasinghe, F. Huang, Y.-B. Cheng, Nano Energy 2 (2013) 174–189.
[14] H.C. Weerasinghe, G.V. Franks, J.D. Plessis, G.P. Simon, Y.B. Cheng, J. Mater. Chem. 20 (2010) 9954–9961.
[15] J.H. Yune, I. Karatchevtseva, G. Triani, K. Wagner, D. Officer, J. Mater. Res. 28 (2013) 488–496.
[16] G. Boschloo, J. Lindstrom, E. Magnusson, A. Holmberg, A. Hagfeldt, J. Photochem. Photobiol. A 148 (2002) 11–15.
[17] F.Z. Huang, D.H. Chen, Q. Li, R.A. Caruso, Y.B. Cheng, Appl. Phys. Lett. (2012) 100.
[18] T. Yamaguchi, N. Tobe, D. Matsumoto, T. Nagai, H. Arakawa, Sol. Energy Mater. Sol. Cells 94 (2010) 812–816.
[19] D. Gutierrez-Tauste, I. Zumeta, E. Vigil, M.A. Hernandez-Fenollosa, X. Domenech, J.A. Ayllon, J. Photochem. Photobiol. A 175 (2005) 165–171.
[20] D.S. Zhang, H.Y. Hu, L.F. Li, D.L. Shi, J. Nanomater (2008).
[21] J.M. Szeifert, D. Fattakhova-Rohlfing, J. Rathousky, T. Bein, Chem. Mater. 24 (2012) 659–663.
[22] E. Stathatos, Y.J. Chen, D.D. Dionysiou, Sol. Energy Mater. Sol. Cells 92 (2008) 1358–1365.
[23] Y. Li, W. Lee, D.K. Lee, K. Kim, N.G. Park, M.J. Ko, Appl. Phys. Lett. (2011) 98.
[24] Y. Li, K. Yoo, D.-K. Lee, J.Y. Kim, H. Kim, B. Kim, M.J. Ko, Nanoscale 5 (2013) 4711–4719.
[25] S.E. Habas, H.A.S. Platt, M.F.A.M. van Hest, D.S. Ginley, Chem. Rev. 110 (2010) 6571–6594.
[26] J. Perelaer, P.J. Smith, D. Mager, D. Soltman, S.K. Volkman, V. Subramanian, J.G. Korvink, U.S. Schubert, J. Mater. Chem. 20 (2010) 8446–8453.
[27] T. Todorov, D.B. Mitzi, Eur. J. Inor. Chem. (2010) 17–28.
[28] M. Arin, P. Lommens, N. Avci, S.C. Hopkins, K. De Buysser, I.M. Arabatzis, I. Fasaki, D. Poelman, I. Van Driessche, J. Eur. Ceram. Soc. 31 (2011) 1067–1074. [29] D. Hwang, D.Y. Kim, S.Y. Jang, D. Kim, J. Mater. Chem. A 1 (2013) 1228–1238. [30] A. Mills, S. LeHunte, J. Photochem. Photobiol. A 108 (1997) 1–35.

[31] D. Amans, C. Malaterre, M. Diouf, C. Mancini, F. Chaput, G. Ledoux, G. Breton, Y. Guillin, C. Dujardin, K. Masenelli-Varlot, P. Perriat, J. Phys. Chem. C 115 (2011) 5131–5139.
[32] K. Sodeyama, M. Sumita, C. O'Rourke, U. Terranova, A. Isam, L.Y. Han, D.R. Bowler, Y. Tateyama, J. Phys. Chem. Lett. 3 (2012) 472–477.
[33] T. Finke, D. Lingenfelser, K. Bindler, U. Eisele, H. Bockhorn, G. Brunklaus, J. Am. Cer Soc. 92 (2009) 1823–1830.
[34] Q.Y. Qu, H.W. Geng, R.X. Peng, Q. Cui, X.H. Gu, F.Q. Li, M.T. Wang, Langmuir 26 (2010) 9539–9546.
[35] L. Cano, J. Gutierrez, A. Tercjak, J. Phys. Chem. 117 (2013) 1151–1156.
[36] M. Estruga, A. Roig, C. Domingo, J.A. Ayllon, J. Nanopart. Res. (2012) 14.
[37] R.L. Callender, C.J. Harlan, N.M. Shapiro, C.D. Jones, D.L. Callahan, M.R. Wiesner, D.B. MacQueen, R. Cook, A.R. Barron, Chem. Mater. 9 (1997) 2418–2433. [38] Z. Hens, J.C. Martins, Chem. Mater. 25 (2013) 1211–1221.
[39] A.J. Morris-Cohen, M. Malicki, M.D. Peterson, J.W.J. Slavin, E.A. Weiss, Chem. Mater. 25 (2013) 1155–1165.
[40] C. Grote, K.J. Chiad, D. Vollmer, G. Garnweitner, Chem. Commun. 48 (2012) 1464–1466.
[41] S. Ito, T.N. Murakami, P. Comte, P. Liska, C. Gratzel, M.K. Nazeeruddin, M. Gratzel, Thin Solid Films 516 (2008) 4613–4619.